Electronic supporting information (ESI) for the manuscript:

Self-assembly, metal binding ability, and magnetic properties of

dinickel(II) and dicobalt(II) triple mesocates

Marie-Claire Dul, Rodrigue Lescouëzec,* Lise-Marie Chamoreau, Yves Journaux,* Rosa Carrasco,

María Castellano, Rafael Ruiz-García, Joan Cano, Francesc Lloret,* Miguel Julve, Catalina Ruiz-Pérez,

Oscar Fabelo, and Emilio Pardo*

Electronic spectra

The electronic absorption spectra of **4** and **5** in water are compared to that of the proligand Et_2H_2L in THF in Fig. S1. Complexes **4** and **5** exhibit a very strong band in the UV region located at $\lambda_{max} = 250$ ($\varepsilon = 88500$ M^{-1} cm^{-1}) and 255 nm ($\varepsilon = 92000$ M^{-1} cm^{-1}), respectively [Fig. S1(a) and (b)]. This intense UV band is unambiguously assigned to an intraligand (IL) $\pi-\pi^*$ transition within the aromatic benzene ring, which occurs at $\lambda_{max} = 270$ nm ($\varepsilon = 29500$ M^{-1} cm^{-1}) for Et_2H_2L with approximately one third-fold intensity relative to that in **4** and **5** as expected from the ligand/metal molar ratio of 3:2 [Fig. S1(c)]. In addition, **4** and **5** show several characteristic d–d bands in the visible and NIR regions.

Complex **4** shows a weak NIR band located at $\lambda_{max} = 945$ nm ($\varepsilon = 35$ M^{-1} cm^{-1}) and a visible band at $\lambda_{max} = 635$ nm ($\varepsilon = 60$ M^{-1} cm^{-1}), which is responsible for its green color [Fig. S1(a)]. These two d–d bands are assigned to the $^3T_{2g}(F) \leftarrow {}^3A_{2g}(F)$ (ν_1) and $^3T_{1g}(F) \leftarrow {}^3A_{2g}(F)$ (ν_2) transitions respectively, of the octahedral high-spin d^8 Ni^{II} ion (O_h point group).[1] The third spin-allowed d–d band corresponding to the $^3T_{1g}(P) \leftarrow {}^3A_{2g}(F)$ (ν_3) transition appears as a poorly resolved shoulder at λ_{max} *ca.* 375 nm ($\varepsilon = 280$ M^{-1} cm^{-1}) in the low-energy tail of the intense UV band. Instead, the extremely weak absorption feature at $\lambda_{max} = 788$ nm ($\varepsilon = 25$ M^{-1} cm^{-1}) is often ascribed to the spin-forbidden d–d band corresponding to the $^1E_g(F) \leftarrow {}^3A_{2g}(F)$ transition of octahedral high-spin d^8 Ni^{II} ion (O_h point group).[1]

Complex **5** shows a weak NIR band at $\lambda_{max} = 1045$ nm ($\varepsilon = 15$ M^{-1} cm^{-1}) and a visible band at $\lambda_{max} = 510$ nm ($\varepsilon = 100$ M^{-1} cm^{-1}), which is responsible for its pink color [Fig. S1(b)]. These two d–d bands are commonly assigned to the $^4T_{2g}(F) \leftarrow {}^4T_{1g}(F)$ (ν_1) and $^4T_{1g}(P) \leftarrow {}^4T_{1g}(F)$ (ν_2) transitions respectively, of the octahedral high-spin d^7 Co^{II} ion (O_h point group).[1] The third spin-allowed d–d band which corresponds to the $^4A_{2g}(F) \leftarrow {}^4T_{1g}(F)$ (ν_3) transition, being essentially a two-electron transition from $(t_{2g})^5(e_g)^2$ to $(t_{2g})^3(e_g)^4$ configurations, is expected to be weak and probably not observed.[1] In fact, the fine structure of the main visible band at $\lambda_{max} = 510$ nm, with two distinct shoulders at $\lambda_{max} = 473$ and 543 nm ($\varepsilon = 90$ M^{-1} cm^{-1}), may likely arise from the term splitting of the $^4T_{1g}(P) \leftarrow {}^4T_{1g}(F)$ (ν_2)

(1) (*a*) E. Koenig, *Struct. Bond.*, 1972, **9**, 175; (*b*) Y. S. Dou, *J. Chem. Ed.*, 1990, **67**, 134.

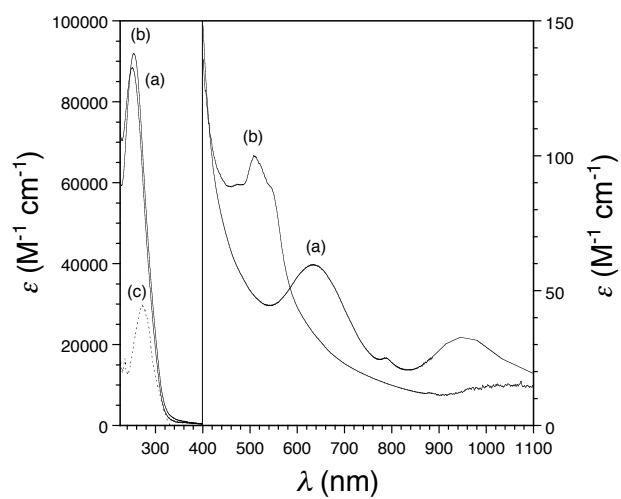transition due to spin-orbit coupling and/or trigonal distortion of the octahedral geometry.

Fig. S1 UV-visible-NIR spectra of **4** (a) and **5** (b) in water and of Et_2H_2L in THF (c).

Magnetic properties

The $\chi_M T$ *vs. T* plots (χ_M being the molar magnetic susceptibility per dinuclear unit and *T* the temperature) of **4** and **5** are compared in Fig. S2.

The $\chi_M T$ *vs. T* plot for **4** is characteristic of moderately weak ferromagnetically coupled Ni^{II}_2 units with a nonnegligible zero-field splitting (ZFS) of the six-coordinate, octahedral high-spin d^8 Ni^{II} ions ($^3A_{2g}$) (Fig. S2). At room temperature, the $\chi_M T$ value of 2.32 cm^3 mol^{-1} K is close to that expected for two magnetically non-interacting high-spin Ni^{II} ions [$\chi_M T = 2 \times (N\beta^2 g_{Ni}^2/3k)S_{Ni}(S_{Ni} + 1) = 2.31$ cm^3 mol^{-1} K with $S_{Ni} = 1$ and $g_{Ni} = 2.15$]. Upon cooling, $\chi_M T$ continuously increases to reach a maximum of 3.21 cm^3 mol^{-1} K at 3.8 K, and then it sligthly decreases down to 3.04 cm^3 mol^{-1} K at 2.0 K. The increase of $\chi_M T$ in the high-temperature region indicates a weak ferromagnetic intradimer interaction. Yet the maximum value of $\chi_M T$ is slightly below than that expected for a ground quintet spin state for the Ni^{II}_2 unit [$\chi_M T = (N\beta^2 g^2/3k)S(S + 1) = 2N\beta^2 g^2/k = 3.47$ cm^3 mol^{-1} K with $S = 2$ and $g = g_{Ni} = 2.15$]. The slight decrease of $\chi_M T$ in the low-temperature region is most likely due to ZFS effects. In fact, the antiferromagnetic interdimer interactions through the diamagnetic Na^I ions are certainly negligible given the large intermolecular metal-metal separation of *ca.* 8 Å.

The magnetic susceptibility data of **4** were analyzed through a spin Hamiltonian for a dimer model which takes into account the axial ZFS of the $^3A_{2g}$ ground state of the octahedral high-spin Ni^{II} ions [eqn (S1) with $S_1 = S_2 = S_{Ni} = 1$], where *J* is the magnetic coupling parameter, *D* is the single-ion axial magnetic anisotropy parameter, and *g* is the Landé factor.[2] A good fit was obtained through the appropriate analytical expression[2b] with $J = +3.6$ cm^{-1}, $D = -3.5$ cm^{-1}, and $g = 2.14$ (solid line in Fig. S2). The calculated values of *J* and *D* for **4** agree with those found for **2** ($J = +3.2$ cm^{-1} and $D = -3.4$ cm^{-1}).[3]

(2) (*a*) A. P. Ginsberg, R. L. Martin, R. W. Brookes and R. C. Sherwood, *Inorg. Chem.,* 1972, **11**, 2884; (*b*) G. De Munno, M. Julve and F. Lloret, *J. Chem. Soc., Dalton Trans.,* 1993, 1179.

(3) D. Cangussu, E. Pardo, M.-C. Dul, R. Lescouëzec, P. Herson, Y. Journaux, E. F. Pedroso, C. L. M. Pereira, H. O. Stumpf, M. C. Muñoz, R. Ruiz-García, J. Cano, M. Julve and F. Lloret, *Inorg. Chim. Acta,* 2008, **361**, 3394.

$$\mathbf{H} = -J\,\mathbf{S_1} \cdot \mathbf{S_2} + D\sum_{i=1,2} \mathbf{S_{zi}}^2 + g\beta H \sum_{i=1,2} \mathbf{S_i} \tag{S1}$$

The $\chi_M T$ *vs. T* plot for **5** agrees with a weak ferromagnetically coupled Co^{II}_2 units with an important spin-orbit coupling (SOC) of the octahedral high-spin d^7 Co^{II} ions ($^4T_{1g}$) (Fig. S2). At room temperature, the $\chi_M T$ value of 5.98 cm^3 mol^{-1} K is close to that expected for two magnetically non-interacting high-spin Co^{II} ions with an important orbital contribution, as compared with the spin-only value [$\chi_M T = 2 \times$ $(N\beta^2 g_{Co}^2/3k)S_{Co}(S_{Co} + 1)$ = 3.75 cm^3 mol^{-1} K with S_{Co} = 3/2 and g_{Co} = 2.0]. Upon cooling, $\chi_M T$ continuously decreases to reach a minimum of 3.90 cm^3 mol^{-1} K at 12.0 K, and then it sligthly increases up to 4.43 cm^3 mol^{-1} K at 2.0 K. The increase of $\chi_M T$ in the low-temperature region is indicative of a weak ferromagnetic intradimer interaction, whereas the decrease of $\chi_M T$ in the high-temperature region is due to the SOC of the orbitally degenerate, high-spin Co^{II} ion in a distorted octahedral coordination geometry, as found in related mononuclear high-spin octahedral cobalt(II) complexes.[4]

The magnetic susceptibility data of **5** were analyzed through a spin Hamiltonian for a dimer model which includes the SOC of the $^4T_{1g}$ ground state of the octahedral high-spin Co^{II} ions, together with the splitting of the T_{1g} orbital term into a singlet (A_1) and a doublet (E) terms due to the axial distortion [eqn (S2) with $S_1 = S_2 = S_{Co}$ = 3/2 and $L_1 = L_2 = L_{Co}$ = 1], where J is the magnetic coupling parameter, λ is the spin-orbit coupling parameter, Δ is the axial orbital splitting, and α is an orbital reduction factor defined as $\alpha = A\kappa$.[3] The κ parameter considers the reduction of the orbital momentum caused by covalency effects ($0 < \kappa \leq 1$), while the A parameter takes into account the admixture between the excited $^4T_{1g}(P)$ and the ground $^4T_{1g}(F)$ levels when using the T_1 and P term isomorphism (A varies between 1.0 and 1.5 for the strong and weak crystal field limits, respectively).[4]

$$\mathbf{H} = -J\,\mathbf{S_1} \cdot \mathbf{S_2} + \alpha\lambda \sum_{i=1,2} \mathbf{L_i} \cdot \mathbf{S_i} + \Delta \sum_{i=1,2} \mathbf{L_{zi}}^2 + \beta H \sum_{i=1,2} (\alpha\mathbf{L_i} + g_e\mathbf{S_i}) \tag{S2}$$

A good fit was obtained by full-matrix diagonalization techniques[5] with $J = +1.1$ cm^{-1}, $\lambda = -132$ cm^{-1}, $\Delta = 109$ cm^{-1}, and $\alpha = A\kappa = 1.10$ (solid line in Fig. S2). The value of A can be calculated from the

---

(4) F. Lloret, M. Julve, J. Cano, R. Ruiz-García and E. Pardo, *Inorg. Chim. Acta*, 2008, **361**, 3432.

(5) J. Cano, *VPMAG package*, University of Valencia, Valencia, Spain, 2003.

crystal field parameters obtained from the analysis of the electronic spectrum of **5** through eqn (S3) and (S4) ($Dq = 10725$ cm^{-1} and $B = 745$ cm^{-1}).[1] The calculated A value is 1.37 and then $\kappa = 0.79$.

$$A = (1.5 - c^2)/(1 + c^2) \tag{S3}$$

$$c = 0.75 + 1.875(B/Dq) - [1 + 1.8(B/Dq) + 2.25(B/Dq)^2]^{1/2} \tag{S4}$$

The calculated values of J, λ, Δ, and κ for **5** agree with those found for **3** ($J = +1.0$ cm^{-1}, $\lambda = -116.3$ cm^{-1}, $\Delta = 108$ cm^{-1}, and $\kappa = 0.79$ with $A = 1.4$).[4] The absolute values of the spin-orbit coupling parameter for these dicobalt(II) triple mesocates are indeed lower than that of the free ion ($\lambda = -180$ cm^{-1}) because of the metal-ligand covalency. Likewise, the strongly reduced values of the orbital reduction parameter reveal a large covalency of the M–N and M–O bonds (to be compared with $\kappa = 1$ for the free ion), which is ultimately responsible for the strong delocalization of the spin density of the metal onto the phenylenediamidate bridges.
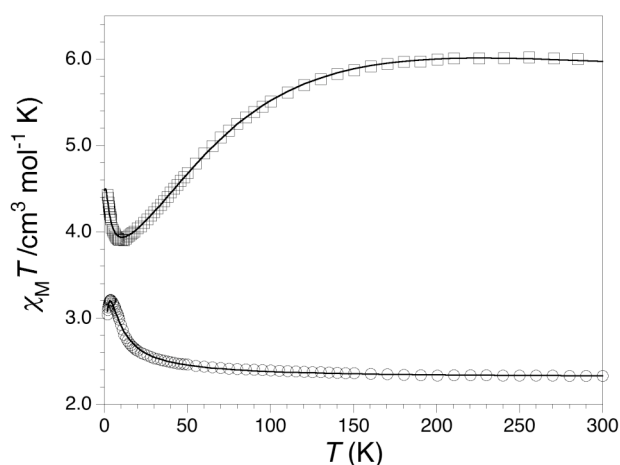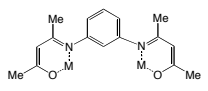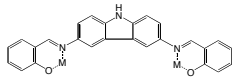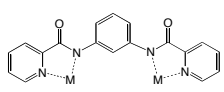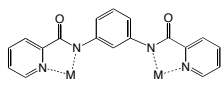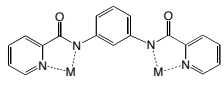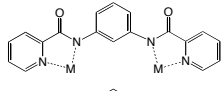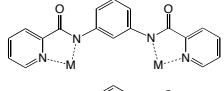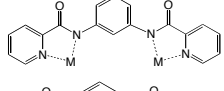

Fig. S2 Temperature dependence of $\chi_M T$ for **4** (○) and **5** (□). The solid lines are the best fit curves.

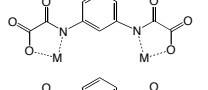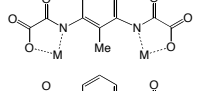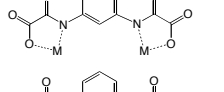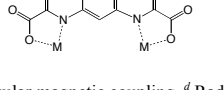**Table S1** Selected magnetostructural data for double- and triple-stranded, dinuclear helicates and mesocates of late and middle 3d metal ions with coordinating group-substituted aromatic diamines, diimines, and diamides as bridging ligands.

Entry	Complex	Type	Topology	M	Geometry	L	d^a / Å	J^b/cm^{-1}	Ref.
1	Na$_4$[Cu$_2$L$_2$] · 18H$_2$O	mesocate	double	Cu^{II} (d^9)	O_h/D_{4h}		6.93	< 1.0	16a
2	Na$_4$[Cu$_2$L$_2$] · 20H$_2$O	mesocate	double	Cu^{II} (d^9)	O_h/D_{4h}		n.a.	< 1.0	16b
3	Na$_4$[Ni$_2$L$_2$] · 15H$_2$O	mesocate	double	Ni^{II} (d^8, hs)	O_h		6.95	−1.4	16b
4	Na$_4$[Co$_2$L$_2$] · 12H$_2$O	mesocate	double	Co^{II} (d^7, hs)	O_h		n.a.	−0.9	16b
5	Na$_4$[Mn$_2$L$_2$] · 10H$_2$O	mesocate	double	Mn^{II} (d^5, hs)	O_h		n.a.	−0.4	16b
6	[Cu$_2$L$_2$] · 2CHCl$_3$	mesocate	double	Cu^{II} (d^9)	T_d/D_{4h}		7.44	−1.0	16c
7	[Cu$_2$L$_2$]	mesocate	double	Cu^{II} (d^9)	T_d/D_{4h}		n.a.	−0.9	16c
8	[Cu$_2$L$_2$]	mesocate	double	Cu^{II} (d^9)	T_d/D_{4h}		n.a.	−1.1	16c
9	[Ni$_2$L$_2$] · 3H$_2$O	mesocate	double	Ni^{II} (d^8, hs)	T_d		n.a.	−2.8	16c
10	[Ni$_2$L$_2$] · 3H$_2$O	mesocate	double	Ni^{II} (d^8, hs)	T_d		n.a.	−2.7	16c
11	[Ni$_2$L$_2$]	mesocate	double	Ni^{II} (d^8, hs)	T_d		n.a.	−2.9	16c
12	[Co$_2$L$_2$] · CHCl$_3$	mesocate	double	Co^{II} (d^7, hs)	T_d		7.26	−1.3	16c
13	[Co$_2$L$_2$] · 4H$_2$O	mesocate	double	Co^{II} (d^7, hs)	T_d		n.a.	−1.2	16c
14	[Co$_2$L$_2$]	mesocate	double	Co^{II} (d^7, hs)	T_d		n.a.	−1.4	16c
15	[Fe$_2$L$_2$(NO$_3$)$_2$]	mesocate	double	Fe^{III} (d^5, hs)	O_h		7.90	+0.4	16d
16	[Cu$_2$L$_2$] · 2MeCN	helicate	double	Cu^{II} (d^9)	T_d		12.02	−0.025^c	17
17	Li$_4$[Cu$_2$L$_2$] · 10H$_2$O	mesocate	double	Cu^{II} (d^9)	D_{4h}		n.a.	−95	18a
18	Na$_4$[Cu$_2$L$_2$] · 11H$_2$O	mesocate	double	Cu^{II} (d^9)	D_{4h}		7.91	−81	18a
19	(Ph$_4$P)$_4$[Cu$_2$L$_2$] · 8H$_2$O	mesocate	double	Cu^{II} (d^9)	D_{4h}		n.a.	−94	18a
20	Li$_4$[Cu$_2$L$_2$] · 12H$_2$O	mesocate	double	Cu^{II} (d^9)	D_{4h}		n.a.	−11.5	18a

21	Na$_4$[Cu$_2$L$_2$] · 12H$_2$O	mesocate	double	Cu^{II} (d^9)	D_{4h}		12.19	−9.5	18a
22	(Bu$_4$N)$_4$[Cu$_2$L$_2$] · 10H$_2$O	mesocate	double	Cu^{II} (d^9)	D_{4h}		n.a.	−8.7	18a
23	Li$_4$[Cu$_2$L$_2$] · 12H$_2$O	mesocate	double	Cu^{II} (d^9)	D_{4h}		n.a.	−20.5	18b
24	(Ph$_4$P)$_4$[Cu$_2$L$_2$] · 8H$_2$O	mesocate	double	Cu^{II} (d^9)	D_{4h}		8.33	−20.7	18b
25	Li$_4$[Cu$_2$L$_2$] · 12H$_2$O	mesocate	double	Cu^{II} (d^9)	D_{4h}		n.a.	−21.2	18b
26	(Ph$_4$P)$_4$[Cu$_2$L$_2$] · 4H$_2$O	mesocate	double	Cu^{II} (d^9)	D_{4h}		n.a.	−23.0	18b
27	(Bu$_4$N)$_4$[Cu$_2$L$_2$]	mesocate	double	Cu^{II} (d^9)	D_{4h}		12.48	−23.9	18c
28	[Co$_2$L$_3$]	mesocate	triple	Co^{III} (d^6, ls)	O_h		6.73	−21.1^d	19a
29	[Fe$_2$L$_3$]	mesocate	triple	Fe^{III} (d^5, hs)	O_h		6.90	−11.0^d	19a
30	[Mn$_2$L$_3$]	mesocate	triple	Mn^{IV} (d^3)	O_h		6.75	n.a.^{d}	19b
31	[Cu$_2$L$_2$]	mesocate	double	Cu^{II} (d^9)	D_{4h}		6.70	n.a.^{e}	20a
32	[Ni$_2$L$_2$]	mesocate	double	Ni^{II} (d^8, ls)	D_{4h}		n.a.		20a
33	[Co$_2$L$_3$]	mesocate	triple	Co^{III} (d^6, ls)	O_h		6.72	+26^d	20a
34	[Fe$_2$L$_3$]	mesocate	triple	Fe^{III} (d^5, hs)	O_h		6.92	n.a.^{d}	20a
35	[Cr$_2$L$_3$]	mesocate	triple	Cr^{III} (d^3)	O_h		n.a.	n.a.^{e}	20a
36	[Mn$_2$L$_3$]	mesocate	triple	Mn^{IV} (d^3)	O_h		6.76	−6.5^d	20b
37	[Fe$_2$L$_3$](PF$_6$)$_4$	helicate	triple	Fe^{II} (d^6, hs)	O_h		11.40	n.a.^{f}	21
38	[Fe$_2$L$_3$](BF$_4$)$_4$	helicate	triple	Fe^{II} (d^6, hs)	O_h		11.56	n.a.^{f}	21
39	[Fe$_2$L$_3$](ClO$_4$)$_4$	helicate	triple	Fe^{II} (d^6, hs)	O_h		11.58	n.a.^{f}	21
40	[Ni$_2$L$_3$](PF$_6$)$_4$	helicate	triple	Ni^{II} (d^8, hs)	O_h		11.54	< 1.0	21
41	[Co$_2$L$_3$](PF$_6$)$_4$	helicate	triple	Co^{II} (d^7, hs)	O_h		11.54	< 1.0	21
42	[Mn$_2$L$_3$](PF$_6$)$_4$	helicate	triple	Mn^{II} (d^5, hs)	O_h		11.66	< 1.0	21

43	$[Cu_2L_2]$	mesocate	double	Cu^{II} (d^9)	D_{4h}/T_d		7.27	+14.6	22a
44	$[Cu_2L_2] \cdot 2CHCl_3 \cdot 2H_2O$	mesocate	double	Cu^{II} (d^9)	D_{4h}/T_d		10.78	−2.2	22b
45	$[Cu_2L_2] \cdot 2H_2O$	mesocate	double	Cu^{II} (d^9)	D_{4h}/T_d		7.56	+21.1	23a
46	$[Ni_2(HL)_3]PF_6 \cdot 21H_2O$	mesocate	triple	Ni^{II} (d^8, hs)	O_h		6.93	+3.6	23a
47	$[Co(H_2O)_6][Ni_2L_3] \cdot THF \cdot 10H_2O$	mesocate	triple	Ni^{II} (d^8, hs)	O_h		6.92	+3.6	23a
48	$[Ag_2(H_2O)][Ni_2L_3] \cdot 11H_2O$	mesocate	triple	Ni^{II} (d^8, hs)	O_h		6.96	+2.9	23a
49	$[Ni_2(HL)_3]ClO_4 \cdot 15H_2O$	mesocate	triple	Ni^{II} (d^8, hs)	O_h		6.93	+3.1	23b
50	$[Co_2L_3] \cdot 19H_2O$	mesocate	triple	Co^{III} (d^6, ls)	O_h		6.85		23b
51	$Na_4[Cu_2L_2] \cdot 10H_2O$	mesocate	double	Cu^{II} (d^9)	D_{4h}		6.82	+16.0	25
52	$(Bu_4N)_4[Cu_2L_2] \cdot 4H_2O$	mesocate	double	Cu^{II} (d^9)	D_{4h}/T_d		7.20	+16.4	13i
53	$Li_4[Ni_2L_3] \cdot 28H_2O$	mesocate	triple	Ni^{II} (d^8, hs)	O_h		6.86	+3.2	26b
54	$Li_4[Co_2L_3] \cdot 37H_2O$	mesocate	triple	Co^{II} (d^7, hs)	O_h		6.85	+1.0	26a,b

[a] Intermetallic distance. [b] Magnetic coupling parameter ($H = -J S_1 \cdot S_2$ with $S_1 = S_2 = S_M$). [c] Intermolecular magnetic coupling. [d] Radical-radical coupling.

[e] Metal-radical coupling. [f] Spin crossover magnetic behavior.